

Statistical representation of high-dimensional deformation fields with application to statistically constrained 3D warping

Zhong Xue ^{*}, Dinggang Shen, Christos Davatzikos

Section of Biomedical Image Analysis (SBIA), Department of Radiology, University of Pennsylvania, 3600 Market Street, Suite 380, Philadelphia, PA 19104, United States

Received 14 January 2006; received in revised form 3 May 2006; accepted 23 June 2006
Available online 2 August 2006

Abstract

This paper proposes a 3D statistical model aiming at effectively capturing statistics of high-dimensional deformation fields and then uses this prior knowledge to constrain 3D image warping. The conventional statistical shape model methods, such as the active shape model (ASM), have been very successful in modeling shape variability. However, their accuracy and effectiveness typically drop dramatically in high-dimensionality problems involving relatively small training datasets, which is customary in 3D and 4D medical imaging applications. The proposed statistical model of deformation (SMD) uses wavelet-based decompositions coupled with PCA in each wavelet band, in order to more accurately estimate the pdf of high-dimensional deformation fields, when a relatively small number of training samples are available. SMD is further used as statistical prior to regularize the deformation field in an SMD-constrained deformable registration framework. As a result, more robust registration results are obtained relative to using generic smoothness constraints on deformation fields, such as Laplacian-based regularization. In experiments, we first illustrate the performance of SMD in representing the variability of deformation fields and then evaluate the performance of the SMD-constrained registration, via comparing a hierarchical volumetric image registration algorithm, HAMMER, with its SMD-constrained version, referred to as SMD+HAMMER. This SMD-constrained deformable registration framework can potentially incorporate various registration algorithms to improve robustness and stability via statistical shape constraints.

© 2006 Elsevier B.V. All rights reserved.

Keywords: Statistical shape model; Active shape model; Shape statistics; Wavelet packet transform; Deformable registration

1. Introduction

Representing prior statistical knowledge of high-dimensional scalar or vector fields is of fundamental importance in a variety of scientific areas including computational anatomy, shape analysis, pattern recognition, and hypothesis testing applied to images or their deformations (Cootes et al., 1994, 1995; Staib and Duncan, 1992; Miller et al., 1997). For instance, statistical study of deformations can be used to provide voxel-based morphological (VBM) characterization of different groups (Ashburner and Friston, 2000); to incorporate prior knowledge of deformations

from training samples into image segmentation and registration algorithms (Twining et al., 2005); to provide an efficient way of synthesizing new deformation fields for validation of registration and segmentation methods (Xue et al., 2005); to regularize deformations according to prior knowledge of sample deformations; and to estimate the missing parts of a deformation from the parts that are observed. In fact, all these applications and the plethora of automated methods for deformable registration of brain images have necessitated the construction of a statistical model that effectively captures the prior distribution of high-dimensional deformation fields, in order to represent the true and full range of anatomical variability.

The goal of this paper is therefore to construct a statistical model of deformation fields from a limited number of training samples. Although many statistical shape

^{*} Corresponding author.

E-mail address: zhong.xue@uphs.upenn.edu (Z. Xue).

modeling methods have been proposed in literature, they are often designed for 2D or 3D shapes that can be represented by a relatively small number of landmarks or outline points (Cootes et al., 1994, 1995). However, the high dimensionality of a variety of image warping methods of 3D structural images renders global PCA-based methods unable to properly estimate the statistics of deformation fields from the typically limited number of training samples (Mallat, 1998). This is especially true for the finer local detail of a deformation field. In this paper, we propose a statistical model of deformation (SMD) that captures the statistics of deformation fields between different individuals. The basic premise throughout the paper is that a number of deformation fields defined in the standard template image domain are available to be used for training, *i.e.* for estimation of the probability density function (pdf) of a high-dimensional deformation field. Defining training samples is not an easy issue, and its full treatment is beyond the scope of this paper. For the purposes of demonstrating and testing our methodology, we used a number of deformations that were obtained using the high-dimensional deformable registration method, called HAMMER (Shen and Davatzikos, 2002). This inevitably biases the generated deformations toward the family of deformations that can be generated by this particular warping algorithm. This is in agreement with our goal here, which is to construct effective statistical priors for constraining a deformable registration mechanism, *i.e.* a procedure that can be applied in conjunction with any registration algorithm. We show that the performance of this registration algorithm is further improved after constraining it by this statistical model; the same could turn out to be true for other registration algorithms. Moreover, training samples can ultimately be generated from first extensively labeling and landmarking a number of images (Boesen et al., 2005), and then applying the high-dimensional warping algorithms to these images, where these labels and landmarks act as the constraints of the deformation fields. Such adequately constrained warping algorithms are likely to generate deformations that are close enough to a gold standard, and therefore appropriate for training.

Estimating the pdf of deformation fields from a limited number of training samples is a very challenging task. One of the most popular methods has been the application of the principal component analysis (PCA) (Cootes et al., 1995, 1998; Moghaddam and Pentland, 1997), in order to estimate a number of principal components that are frequently called principal modes of variation. However, this approach fails dramatically when applied to 3D dense deformation fields, due to under-training in practical settings. For example, accurately estimating a dense 3D deformation field of the entire brain could require tens of thousands of training deformations, if not more. The dramatic failure of standard methods for estimating covariance matrices and the associated pdfs has been well-known in the signal estimation literature (Mallat, 1998). Accordingly, in the 1990s, methods based on scale-space decompo-

sitions were investigated. Our approach, referred to as SMD, builds upon the methods described in Davatzikos et al. (2003a,b), Coifman and Wickerhauser (1992), Mohamed and Davatzikos (2004); which uses wavelet-based decompositions coupled with PCA in each wavelet band, in order to more accurately estimate pdfs of high-dimensional deformation fields, when only a relatively small number of training samples are available (*e.g.* tens, or in the order of 100).

After obtaining SMD, we use it as prior knowledge to constrain the deformable registration. Compared to conventional registration methods which assume some generic smoothness of deformation fields, the SMD-constrained deformable registration can achieve more robust performance, because the regularization constraints reflect the relatively complex nature of the respective deformation fields. Our experiments first compare SMD with the conventional global PCA method. Then, the performance of the SMD-constrained registration is evaluated by comparing the high-dimensional deformable registration method, HAMMER, with its SMD-constrained version, referred to as SMD+HAMMER, via registering simulated and real MR brain images.

The rest of the paper is organized as follows: Section 2 describes the statistical model of deformations and the SMD-constrained registration framework in detail. Experiments are carried out in Section 3. At last, Section 4 concludes the results.

2. Methods

In this section, we first describe how to use statistical model of deformation (SMD) to estimate the statistics of high-dimensional deformation fields that reflect inter-individual variability of brain structures. Then the framework of SMD-constrained registration is introduced in detail.

2.1. Statistical model of deformation

2.1.1. Description of SMD

Denoting $\mathbf{f}(\mathbf{x})$ as the deformation field defined in the template image domain Ω_t , $\mathbf{x} \in \Omega_t$, the objective is to estimate the pdf of \mathbf{f} , *i.e.* $p(\mathbf{f})$, from a relatively small number of training samples. The commonly used PCA method (*e.g.* Cootes et al., 1994; Miller et al., 1997) fails miserably when \mathbf{f} is of very high dimensionality. This is because a global PCA model is able to capture mainly global size and shape characteristics that are of limited interest and value, especially for capturing the variability of complex deformations. In order to capture finer and more localized variations of \mathbf{f} , we follow and extend the framework proposed in Davatzikos et al. (2003a), which is referred to as the wavelet-based PCA (W-PCA) model. The W-PCA model decomposes \mathbf{f} using the wavelet-packet transform (WPT) and subsequently captures within-scale statistics via hierarchically organized PCA models. These PCA models are estimated from statistical distributions that are both of

lower dimensionality, and more compact due to correlations among variables (*e.g.* the PCA model derived from a high-scale representation of \mathbf{f} represents a very compact distribution due to the smoothing and down-sampling applied at each level of the wavelet-packet decomposition; the distribution of high frequency detail within a local window is also easier to estimate due to its low dimensionality owing to the small window size). Performing PCA within each band at a given scale is important, due to correlations among wavelet coefficients corresponding to adjacent locations, something which is particularly prominent in smooth elastic-type of deformations, in contrast to, for example, acoustic signals in which wavelet coefficients are typically assumed to be statistically independent. The fundamental assumption in W-PCA is that the wavelet-based rotation renders the covariance matrix of \mathbf{f} close to block-diagonal, thereby enabling a more accurate estimation from a limited set of examples, compared to the usual sample covariance estimation.

In theory, if the W-PCA model described above captures the statistics of deformation \mathbf{f} accurately, we can just use it as the statistical model. In practice, however, the assumption that the covariance matrix of \mathbf{f} is block-diagonal in the wavelet-packet basis does not hold exactly. Although it is well-known that for broad classes of signals, correlations across different scales diminish rapidly, they are nonetheless non-negligible for adjacent scales. In order to alleviate this problem, we observe that additional constraints imposed on the estimated deformation fields can be used to define subspaces in which the deformation must belong to. Therefore, we require that a valid deformation field simultaneously satisfies all available constraints, *i.e.* it belongs to the intersection of a number of subspaces, each of which satisfies some constraints on the deformation. The W-PCA model applied to the deformation field specifies one such subspace.

In order to describe the second subspace, we use the W-PCA model of the Jacobian determinants of the deformation fields, since they reflect local volumes of anatomical structures, which are important from the perspective of spatial distribution of the amount of brain tissue. Fig. 1 highlights two precentral gyri from different subjects, which differ quite dramatically in shape, but not in volume. More generally, it would be reasonable to assume that, although the cortical folding patterns can vary wildly across individuals, the need of different cortical structures to occupy certain tissue volume renders the Jacobian determinant, which is directly related to tissue volume, relatively little variable across individuals, and therefore it would be easier to estimate the statistics of Jacobian determinants from a limited number of samples. It is worth noting that the complementary property of the statistical models of deformation fields and those of the Jacobian determinants allows us to combine them together by requiring that a valid deformation field be within the intersection of the subspaces defined by them. Therefore, a valid deformation field has to be iteratively constrained by both of the statistical models. We

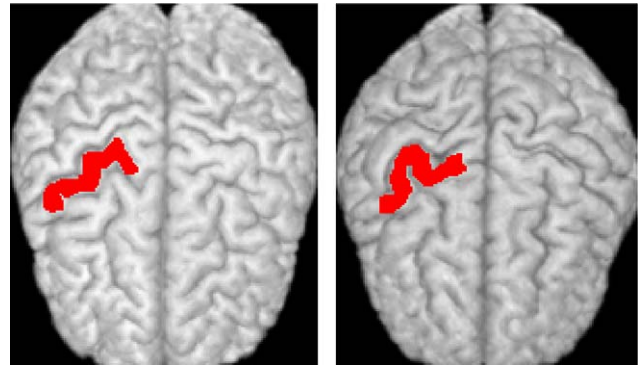


Fig. 1. Jacobian determinants, reflecting volumetric changes, could be conceptually expected to be less variable than the displacement fields. For example, the displacement fields of the precentral gyri are very different for these two brains, whereas the volumes of these gyri are very similar, leading to much less variable Jacobian determinants.

note, here, that converting a constraint on the Jacobian determinant to a constraint on the deformation field, *i.e.* finding the displacement field that satisfies certain conditions on the Jacobian determinant is not straightforward, and it does not have a unique solution. Herein we use Karacali and Davatzikos (2004), which utilizes an iterative projection scheme that minimally, according to some distance criteria, modifies a given displacement field so that it satisfies certain conditions on the Jacobian determinant. This algorithm is used to realize the projection of a given displacement field to the subspace of “valid Jacobians”.

The third subspace is represented by a nested Markov random field (MRF) regularization, which imposes spatial smoothness at different scales in conjunction with the inverse WPT. The purpose of MRF regularization is to eliminate potential discontinuities emanating from the assumption of independence across wavelet bands.

In the following subsections, we first describe the W-PCA model, which can be used to effectively capture the statistics of both deformation fields and their Jacobian determinants. Then, we introduce the MRF regularization in detail. Finally, we summarize the algorithm to regularize deformation fields using SMD.

2.1.2. The wavelet-PCA (W-PCA) models for estimating the pdfs of deformation fields and their Jacobian determinants

The W-PCA model is used to estimate the pdf of deformation fields, *i.e.* $p(\mathbf{f})$, using N samples. It first applies an L -level WPT to \mathbf{f} and then constructs a PCA model of the wavelet coefficients of each wavelet band at level L , and finally it combines the pdfs of difference wavelet bands together. Fig. 2 illustrates the structure of 2-level 1D WPT. For 3D WPT, the wavelet coefficients at level l are represented by $\mathbf{w}^{(l,b)}$, $b = 0, 1, \dots, B_l - 1$, where $B_l = 8^l$ and $l = 1, 2, \dots, L$. At each level, $\mathbf{w}^{(l,0)}$ always represents the low-pass wavelet coefficients. For simplicity, \mathbf{f} is also referred to as $\mathbf{w}^{(0,0)}$.

After L -level WPT, \mathbf{f} can be represented by all the wavelet coefficients at level L , *i.e.* $\mathbf{w}^{(L,b)}$. Assuming that different

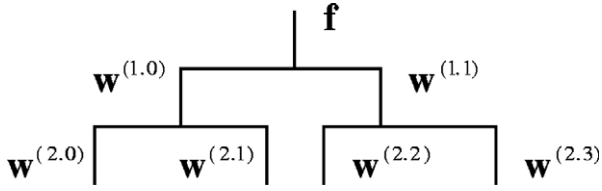


Fig. 2. Wavelet-packet transform (WPT).

bands in the wavelet subspaces are independent, W-PCA estimates the pdf of \mathbf{f} as

$$p_{\text{WPCA}}(\mathbf{f}) = \prod_{b=0}^{B_L-1} p(\mathbf{w}^{(L,b)}). \quad (1)$$

The pdf of each band (L,b) , $p(\mathbf{w}^{(L,b)})$, can be estimated by applying PCA to the wavelet coefficients of N deformation field samples in that wavelet band, denoted as $\mathbf{w}_s^{(L,b)}$, $s = 1, 2, \dots, N$. After performing PCA, we obtain the mean of the wavelet coefficients $\bar{\mathbf{w}}^{(L,b)}$ and the matrix $\Phi^{(L,b)}$ formed by the $K_{(L,b)}$ eigenvectors of the covariance matrix of these wavelet coefficients corresponding to the $K_{(L,b)}$ largest eigenvalues $\lambda_j^{(L,b)}$, $j = 1, \dots, K_{(L,b)}$, of that covariance matrix. Therefore, $\mathbf{w}^{(L,b)}$ can be represented by its projected vector or feature vector $\mathbf{v}^{(L,b)}$ in the space spanned by the $K_{(L,b)}$ eigenvectors,

$$\mathbf{v}^{(L,b)} = \Phi^{(L,b)\top} (\mathbf{w}^{(L,b)} - \bar{\mathbf{w}}^{(L,b)}). \quad (2)$$

Then, the pdf of \mathbf{f} in Eq. (1) is represented by

$$p_{\text{WPCA}}(\mathbf{f}) = \prod_{b=0}^{B_L-1} c_{(L,b)} \exp \left\{ - \sum_{j=1}^{K_{(L,b)}} \frac{v_j^{(L,b)^2}}{2\lambda_j^{(L,b)}} \right\}, \quad (3)$$

where $c_{(L,b)}$ is the normalization coefficient and $v_j^{(L,b)}$ is the j th element of feature vector $\mathbf{v}^{(L,b)}$.

This W-PCA model can not only be applied to deformation fields, but also to the Jacobian determinants of deformations, thus, we can capture the statistics of deformation fields via their Jacobian determinants,

$$p_J(\mathbf{f}) = p_{\text{WPCA}}(J(\mathbf{f})), \quad (4)$$

where $J(\mathbf{f}(\mathbf{x})) = \left| \frac{\partial \mathbf{f}(\mathbf{x})}{\partial \mathbf{x}^\top} \right|$ represents the operator to calculate the Jacobian determinant of a deformation field \mathbf{f} .

We stress the importance of using PCA within each wavelet band, which is in contrast to the commonly used independence assumption for wavelet coefficients. In particular, PCA is known to be the optimal linear expansion, provided that a good estimate of the covariance matrix is available. Although sample covariance is a very inaccurate estimate of the covariance of \mathbf{f} (Davatzikos et al., 2003a), the sample covariance at various scales provides a much better estimate of the covariance at that scale, because of the relatively low dimensionality of each wavelet band (see discussion in Section 2.1.1). As a result, the W-PCA model can capture correlations between adjacent spatial locations at a given scale.

2.1.3. Hierarchical MRF regularization

As mentioned in Section 2.1.1, one W-PCA model of deformation fields does not fully capture the region of valid deformation fields: if deformations are synthesized directly using the W-PCA model, some unrealistic discontinuities emanating from the assumption of independence across wavelet bands may occur. In order to eliminate such potential discontinuities, a nested Markov random field (MRF) regularization scheme that imposes spatial smoothness at different scales is applied in conjunction with the inverse WPT.

Suppose L -level WPT is performed, and let level L be the lowest resolution level, in inverse WPT, all the wavelet bands at level L are used to reconstruct the wavelet coefficients at the higher level $L - 1$. Then, the newly reconstructed low-pass coefficient at level $L - 1$, $\hat{\mathbf{w}}^{(L-1,0)}$, is regularized using MRF, which eliminates the independencies of the wavelet coefficients of different bands at level L . Similarly, all the wavelet coefficients at level $L - 1$ will be used to reconstruct the wavelet coefficients at level $L - 2$ by performing inverse WPT, after which the newly reconstructed low-pass wavelet coefficient at level $L - 2$, $\hat{\mathbf{w}}^{(L-2,0)}$, is regularized using MRF. This eliminates the independencies of the wavelet coefficients of different bands at level $L - 1$. In this way, we repeat the same process from the lowest resolution to the finest resolution. That is, at each level l ($l = L - 1, L - 2, \dots, 0$), after reconstructing all the wavelet coefficients, the low-pass wavelet coefficient at level l , $\hat{\mathbf{w}}^{(l,0)}$, is regularized by performing MRF to eliminate some discontinuity caused by the independencies of those different wavelet bands at level $l + 1$. Finally, the regularizations at different resolution levels propagate to the finest resolution, thus results a hierarchically smoothed deformation field. In the following paragraph, we describe how MRF regularization is performed to a low-pass wavelet coefficient.

Denoting the input low-pass coefficient as $\hat{\mathbf{w}}$ (which can be any of $\hat{\mathbf{w}}^{(l,0)}$, $l = L - 1, \dots, 0$), the MRF regularization estimates a “true” \mathbf{w}_r , by assuming that the low-pass wavelet coefficient forms a MRF and $\hat{\mathbf{w}}$ is a degraded observation of \mathbf{w}_r ($\hat{\mathbf{w}} = \mathbf{w}_r + \mathbf{n}$, where \mathbf{n} is the disturbance assumed to be zero-mean Gaussian noise with standard deviation (std) σ_N), and by using the Maximum *a posteriori* (MAP) framework (Geman and Geman, 1984; Shen and Ip, 1998),

$$\begin{aligned} \mathbf{w}_r &= \operatorname{argmax}_{\mathbf{w}} \{p(\mathbf{w}|\hat{\mathbf{w}})\} \\ &= \operatorname{argmax}_{\mathbf{w}} \{p(\hat{\mathbf{w}}|\mathbf{w})p(\mathbf{w})/p(\hat{\mathbf{w}})\}. \end{aligned} \quad (5)$$

Assuming the prior $p(\mathbf{w})$ and the likelihood $p(\hat{\mathbf{w}}|\mathbf{w})$ are Gaussian distributions, we have $p(\mathbf{w}) \propto \exp\{-\Psi(\mathbf{w})\}$ and $p(\hat{\mathbf{w}}|\mathbf{w}) \propto \exp\left\{-\frac{1}{2\sigma_N^2} \|\mathbf{w} - \hat{\mathbf{w}}\|^2\right\}$, where $\Psi(\mathbf{w}) = \frac{1}{2}(\mathbf{w} - \bar{\mathbf{w}})^\top \chi^{-1}(\mathbf{w} - \bar{\mathbf{w}})$. $\bar{\mathbf{w}}$ and χ refer to the mean and the covariance matrix of \mathbf{w} , respectively, and the structure of χ meets the MRF property. Thus, \mathbf{w}_r is solved by minimizing an energy function, $E_r(\mathbf{w})$,

$$E_r(\mathbf{w}) = \frac{1}{2\sigma_N^2} \|\mathbf{w} - \hat{\mathbf{w}}\|^2 + \Psi(\mathbf{w}). \quad (6)$$

We use a simplified approach similar to Shen and Ip (1998) and Belge et al. (2000) to minimize $E_r(\mathbf{w})$. First, we estimate $p(\mathbf{w})$ as a product of all the local (marginal) pdfs across the locations \mathbf{x} , *i.e.* $p(\mathbf{w}) = \prod_{\mathbf{x}} G(\mathbf{w}_{\mathbf{x}}, \mu_{\mathbf{x}}, \sigma_{\mathbf{x}})$, where $G(\cdot, \cdot, \cdot)$ represents a single Gaussian distribution with mean $\mu_{\mathbf{x}}$ and standard deviation $\sigma_{\mathbf{x}}$. Then $\Psi(\mathbf{w})$ in Eq. (6) is estimated by $\hat{\Psi}(\mathbf{w}) = \sum_{\mathbf{x}} \left\{ \frac{\|\mathbf{w}_{\mathbf{x}} - \mu_{\mathbf{x}}\|^2}{2\sigma_{\mathbf{x}}^2} \right\}$, where $\mu_{\mathbf{x}} = \frac{1}{|\delta(\mathbf{x})|} \sum_{\mathbf{y} \in \delta(\mathbf{x})} \mathbf{w}_{\mathbf{y}}$ and $\sigma_{\mathbf{x}}^2 = \frac{1}{|\delta(\mathbf{x})|-1} \sum_{\mathbf{y} \in \delta(\mathbf{x})} \|\mathbf{w}_{\mathbf{y}} - \mu_{\mathbf{x}}\|^2$. $\delta(\mathbf{x})$ refers to a neighborhood centered on \mathbf{x} but not including \mathbf{x} , and $|\delta(\mathbf{x})|$ is the cardinality of $\delta(\mathbf{x})$. Therefore, the regularized wavelet coefficients \mathbf{w}_r can be obtained by minimizing Eq. (6) using the Newton's method.

2.1.4. Summary of SMD

SMD combines the W-PCA models of deformation fields and their Jacobian determinants, as well as the MRF regularization together, and requires that a valid deformation field locates inside the intersection of the three subspaces defined by these models. Therefore, given an input deformation field, we can use the following steps to iteratively project it onto each of the three subspaces, and finally generate the SMD-regularized deformation field according to the priors. This SMD regularization algorithm is summarized as follows,

- Step 1. Project the deformation field onto the W-PCA model of valid deformation fields.
- Step 2. Project the Jacobian of the deformation field onto the W-PCA model of valid Jacobian determinants.
- Step 3. Find new deformation field whose Jacobian matches the one generated in Step 2, using Karacali and Davatzikos (2004).
- Step 4. Apply the nested MRF regularization to impose spatial smoothness on the deformation at all scales.
- Step 5. Go to step 1 and iterate until the smoothed deformation field belongs to the subspaces of valid Jacobians and deformations.

2.2. SMD-constrained deformable registration

After estimating the statistical model of deformation fields, we can use this prior knowledge to constrain the deformation fields during image registration. The structure of the SMD-constrained deformable registration is shown in Fig. 3. Unlike the traditional registration algorithms, the SMD-constrained registration improves the robustness and stability of the registration results since prior statistical information about the variability of deformation fields has been embedded into the registration procedure.

Particularly, the SMD-constrained deformable registration is achieved by iteratively regularizing the results of a

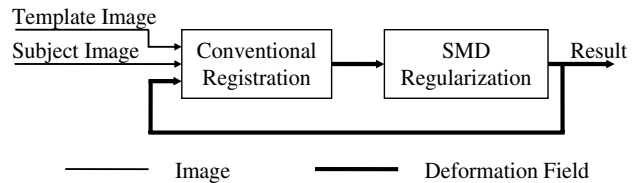


Fig. 3. The structure of the SMD-constrained deformable registration, wherein the deformation from the template to the subject image generated by a conventional registration algorithm is iteratively regularized using SMD.

conventional registration method. Compared to the conventional registration methods that only utilize the smoothness constraint of deformation term and the image-similarity term, the SMD-constrained registration uses a new statistical regularization on the deformation field so that it conforms to the prior knowledge defined by SMD. In the first iteration, we use the registration algorithm to estimate a new deformation field between the template image and the subject image, and then regularize the deformation field using SMD (the SMD regularization algorithm is described in Section 2.1.4); in the subsequent iterations, the regularized deformation field is used as the input of the registration algorithm in order to iteratively refine the registration result. The SMD-constrained registration terminates until the difference between the resultant deformation fields of two subsequent iterations drops below a certain threshold. Since smoothness of deformation field has been imposed from the SMD, in the traditional registration algorithm, a smaller weight for smoothness constraint is chosen, to prevent from over smoothing the deformation field.

In the experiments, we use the HAMMER registration algorithm as the registration part and SMD as the regularization part. This approach is referred to as SMD+HAMMER. Although SMD+HAMMER may not minimize the overall energy function globally, we could generate more robust registration results conforming to the prior knowledge of deformation fields by iteratively regularizing the deformation field estimated by HAMMER, without changing its mechanism. In other words, we treat the family of all possible deformation fields generated by HAMMER as the fourth subspace. Then, the registration result of SMD+HAMMER is obtained by iteratively projecting the current deformation field onto each of the four subspaces until the resultant deformation field locates in the intersection of all these subspaces.

3. Experimental results

In this section, we first show that SMD is more effective in capturing the statistics of high-dimensional deformation fields than the conventional global PCA used by active shape models and related approaches. Evaluation is then performed to illustrate that SMD+HAMMER is more robust than HAMMER in registering both simulated and real MR brain images, without decrease in registration accuracy.

3.1. Performance of SMD in capturing the statistics of deformations

The ability of SMD to capture the statistical variation of deformation fields resulting from brain image warping is first tested by simulating realistic brain images, as well as by measuring generalization ability, *i.e.* ability to represent new samples.

Simulating brain images. Simulated deformations are generated using random sampling from the pdf estimated by SMD. Training was achieved using 158 brain images from the Baltimore longitudinal study of aging (BLSA) (Resnick et al., 2000). Since PCA is performed for each wavelet band in the W-PCA model, we simulate images by randomly selecting the PCA coefficients of different wavelet bands according to their estimated distributions. Fig. 4 shows examples of the images derived from simulated deformations. In this case, the feature vectors of each wavelet band are randomly sampled to be around ± 2 times of the corresponding variances. These simulated images allow us to visually appreciate the characteristics of the deformations captured by SMD.

Generalization. In order to quantitatively evaluate the performance of SMD, we use a generalization measure (Styner et al., 2003) to compare SMD with the conventional global PCA method, by using a leave-one-out cross-validation. First, a statistical model is constructed by leaving one deformation field out of the training set. Then, the left-out deformation field is projected onto the constructed statistical model by using the SMD regularization algorithm in Section 2.1.4, thus obtaining a new deformation field in the statistical space of deformations and also the difference between these two deformation fields. Finally, by averaging all differences on all leave-one-out cases, the generalization error is finally obtained. Low generalization error means good generalization and also implies that the statistical model is not only able to accurately represent the training samples, but also to accurately represent other testing samples. Experimental results show that the average and the standard deviation of the generalization errors are 2.3 and 0.6 mm, respectively, for SMD, which is much smaller than those using conventional PCA (Xue et al., 2005). Therefore, SMD can capture the

statistics of high-dimensional deformation fields more accurately than the conventional global PCA method.

3.2. Performance of SMD-constrained deformable registration

In this subsection, the performance of the SMD-constrained registration (SMD+HAMMER) is evaluated on both simulated and real MR brain images, and it is compared with that of HAMMER. In the first experiment, we examine the ability of the two registration methods to detect morphological differences (atrophy) simulated in two groups of brain scans, by examining quantities extracted from the deformation fields linking a template with each image in these two groups, *i.e.* using a computational anatomy approach (Davatzikos et al., 2001). Moreover, other measurements, such as smoothness of deformation fields, are also compared. Two additional experiments are performed on real data. First, the registration accuracy of each registration method is measured by a number of expert-defined anatomical landmarks. Second, serial images of the same subjects are aligned onto the template space, and the temporal consistency/smoothness of the registration results is measured quantitatively and also visually for each registration method. The premise in the last experiment is that the transformations that yield temporally consistent results are likely to be more accurate, since the input images are acquired from the same individual in consecutive years, and they differ very little from year to year.

3.2.1. Registration of simulated atrophy images

In this experiment, we use both HAMMER and SMD+HAMMER to register the MR brain images of different subjects with and without simulated atrophy. 10 T1-weighted MR brain images of 10 different subjects are used, referred to as the group of original brains. For each original image, we simulate the atrophy on both precentral gyrus and superior temporal gyrus (Davatzikos et al., 2001). Therefore, we obtain 10 images with simulated atrophy, referred to as the group of simulated brains. Fig. 5 shows an example of the original MR brain image and its simulated atrophy image.

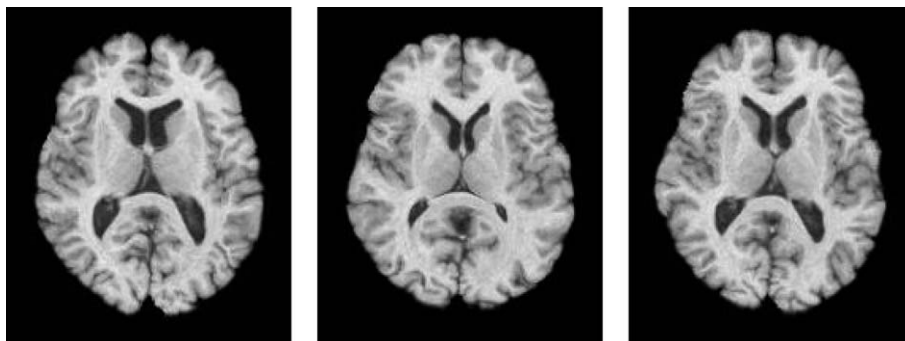


Fig. 4. Examples of randomly simulated images using SMD.

All of these 20 images, *i.e.* 10 in the original group and 10 in the simulated group, are then registered onto the template image by using HAMMER and SMD+HAMMER, respectively. In order to evaluate the performance of the registration results, we perform the following quantitative comparisons.

3.2.1.1. Image intensity difference and smoothness of deformation field. We have used the average image intensity difference and the smoothness of deformation field to evaluate the performance of the registration, since these values give us an idea about the goodness of registration. It should be noted that good registration results obtained from different registration methods should have similar values for both image intensity difference and the smoothness of deformation field. In this paper, the average image intensity difference between the registered subject image and the template image is calculated by

$$e(I_t, I_s, \mathbf{f}) = \frac{1}{|\Omega_t|} \sum_{\mathbf{x} \in \Omega_t} (I_t(\mathbf{x}) - I_s(\mathbf{f}(\mathbf{x})))^2 \quad (7)$$

and the smoothness of deformation field is evaluated using the histogram of the Jacobian determinants, as well as the histogram of the Laplacian magnitudes of that deformation field.

Fig. 6 shows the average image intensity difference between the template image and each registered subject image. It can be seen that the average image intensity difference is similar for both HAMMER and SMD+HAMMER registration results, and there is no significant difference between the results of these two registration methods. That means the registration accuracy is not

decreased by using SMD as additional constraints for deformation field. In addition, it can be observed that the average image intensity difference of affine registration method is always the largest for each subject, as expected. Notice that the average image intensity difference is still large even for the HAMMER and SMD+HAMMER algorithms. This is because the image intensities are not globally normalized between the template and each subject image, when calculating the average image intensity difference.

Figs. 7 and 8 compare the histograms of Jacobian determinants and the histograms of the Laplacian magnitudes of the deformation fields generated by HAMMER and SMD+HAMMER, respectively. It can be seen that for SMD+HAMMER, the Jacobian determinants are more tightly distributed around one, and the Laplacian magnitudes are relatively small, compared to HAMMER.

The resultant deformation fields can also be visually observed in Fig. 9. We can see that HAMMER and SMD+HAMMER generate similar deformation fields for the same template and subject image pair, but the SMD+HAMMER result is relatively smooth. Moreover, we can also see that in some locations pointed by the arrows, the deformation field is clearly regularized by SMD+HAMMER, as compared with the HAMMER result.

All of these results indicate that by incorporating SMD into the registration procedure, we can obtain relatively smooth deformation fields, without decreasing registration accuracy. Further evaluation of registration accuracy is also performed by measuring the accuracy in aligning manual landmarks in real image as provided in Section 3.2.2.

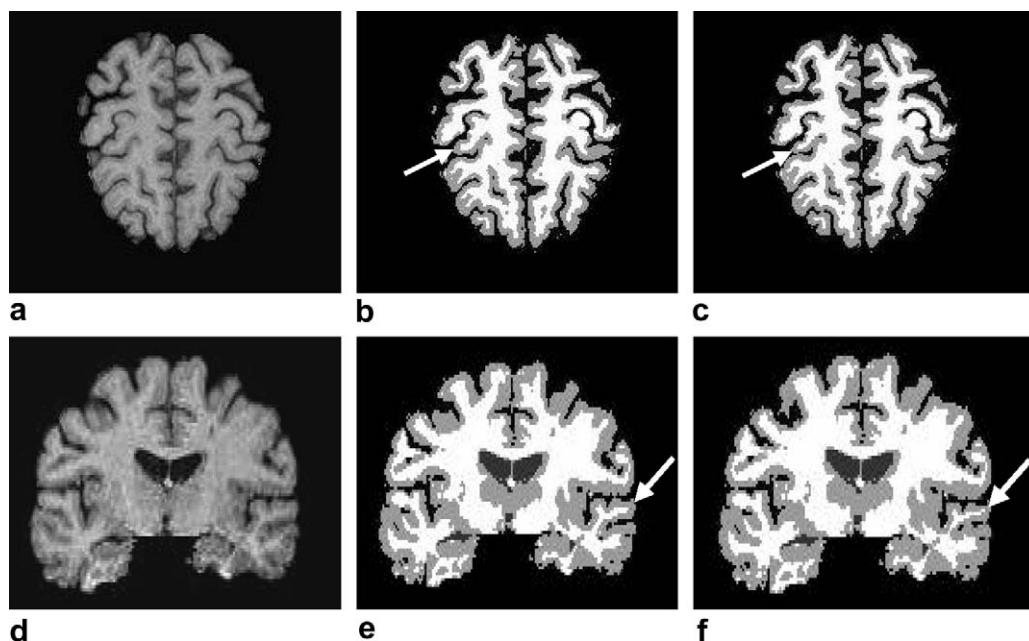


Fig. 5. Examples of the original MR brain image, the segmented image and the simulated image with local atrophy on precentral gyrus and superior temporal gyrus. (a) Original image; (b) segmented image; (c) segmented image with simulated atrophy on precentral gyrus; (d) original image; (e) segmented image; (f) segmented image with simulated atrophy on superior temporal gyrus.

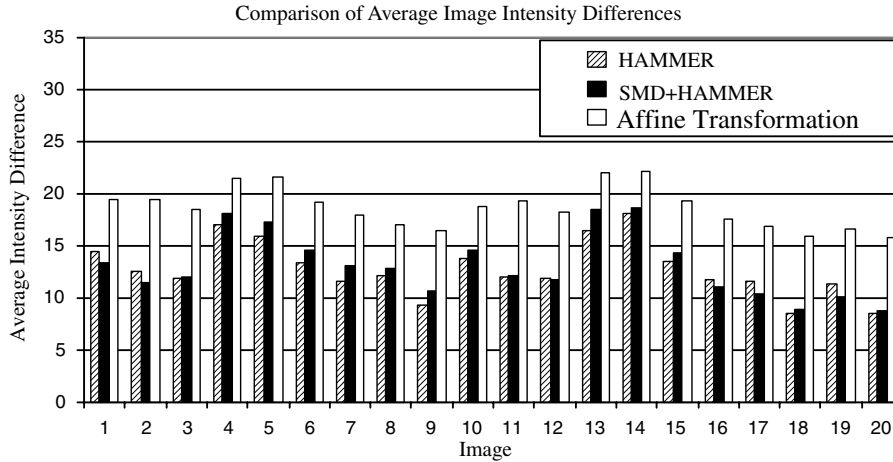


Fig. 6. Comparison of average image intensity difference between the template image and the registered subject images.

3.2.1.2. *Ability of detecting simulated atrophy.* We then used a computational anatomy method to detect group differences between the brains with atrophy and the original ones. In particular, for each brain image, we can calculate the tissue density maps for different brain tissues in the template image space, *i.e.* the RAVENS maps (Resnick et al., 2000; Goldszal et al., 1998; Davatzikos, 1998) of gray matter (GM), white matter (WM), and the cerebrospinal fluid inside the ventricle (VN), from the deformation field that registers this brain onto the template space. These tissue density maps are created in a volume-preserving way, so they directly reflect the regional volumetric structure of the respective brains. For example, if an individual’s ventricles are deformed into conformation with a tem-

plate’s ventricles, local expansion or contraction changes the local density of CSF. Local contraction, *i.e.* trying to match big subject ventricle to the small template ventricle, increases the local density. This is also true for GM and WM structures, as well as for arbitrary subdivisions of them. Since the original information about volumes of brain structures and any arbitrary partitions of them is converted into tissue densities, and since these tissue density maps are registered, local differences or changes in volumes can be quantified by respective changes in the tissue density maps. Fig. 10 shows the examples of the brain tissue density maps for GM, WM, and VN, calculated from HAMMER and SMD+HAMMER results, respectively. It can be seen that relatively smooth tissue density maps were obtained by SMD+HAMMER. Our assumption is that these smooth maps would remove unwanted “noise” and would allow us to better detect the atrophy.

In order to test for group differences, we performed a paired *t*-test on the combined brain density maps of the two groups (each group includes 10 brain density maps calculated from 10 respective deformation fields), using the statistical parametric mapping (SPM) software package. A smaller *p*-value or a larger *t*-value of a paired *t*-test will indicate better separation ability. Table 1 shows the statistical measures for the two clusters detected in the locations of the superior temporal gyrus and the precentral gyrus, respectively. It can be seen that smaller *p*-values (both of $p_{FWE-corr}$ and $p_{FDR-corr}$) and larger *t*-values are obtained for the SMD+HAMMER algorithm. In fact, as shown in Fig. 10, the brain density maps of GM, WM, and VN calculated from SMD+HAMMER results are smoother than those from HAMMER results, which also agrees with the results shown in Figs. 8 and 9. Therefore, SMD+HAMMER in these experiments was much more powerful in detecting group differences.

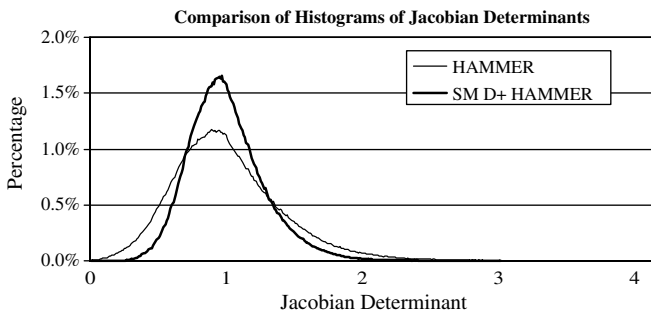


Fig. 7. Comparison of Jacobian determinants of deformation fields.

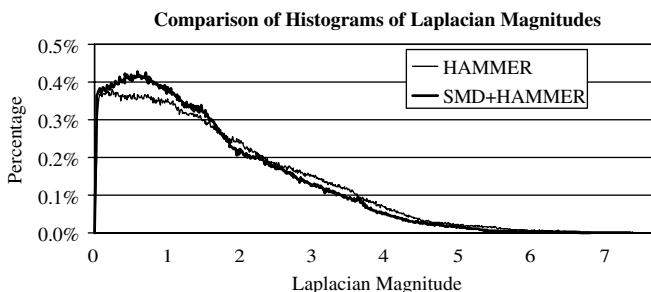


Fig. 8. Comparison of the Laplacian magnitude of deformation fields.

3.2.2. Registration of real MR brain data

3.2.2.1. *Measuring registration accuracy by manual landmarks.* We used 18 MR brain images from different

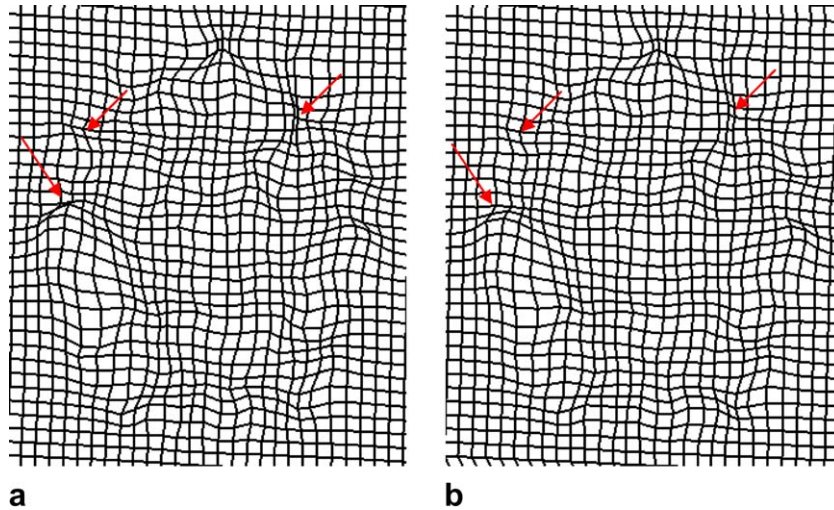


Fig. 9. Examples of the deformation fields generated by HAMMER and SMD+HAMMER, respectively. (a) HAMMER; (b) SMD+HAMMER.

subjects, each of which had 20 landmarks manually marked by experts. After registering these 18 images, we transformed all the manual landmarks onto the template domain and thus obtained 20 groups of corresponding points in the template domain, and each group consists of 18 points of the same landmark from 18 different subject images. For each group, we calculated the mean and std of the distances between all the 18 points and their average point; for ideal registration, these should be zero. These mean and std for each landmark group are shown in

Fig. 11. It can be seen that all the means are below 5 mm, and similar registration accuracy was achieved for HAMMER and SMD+HAMMER (p -value for a paired t -test is 0.023). Although the results of HAMMER and SMD+HAMMER are comparable and they have no significant difference, the registration accuracy on most manual landmarks for HAMMER is slightly higher than that of SMD+HAMMER, this may be because that the SMD trained could not completely represent new deformations, and the resultant deformation fields for new subject

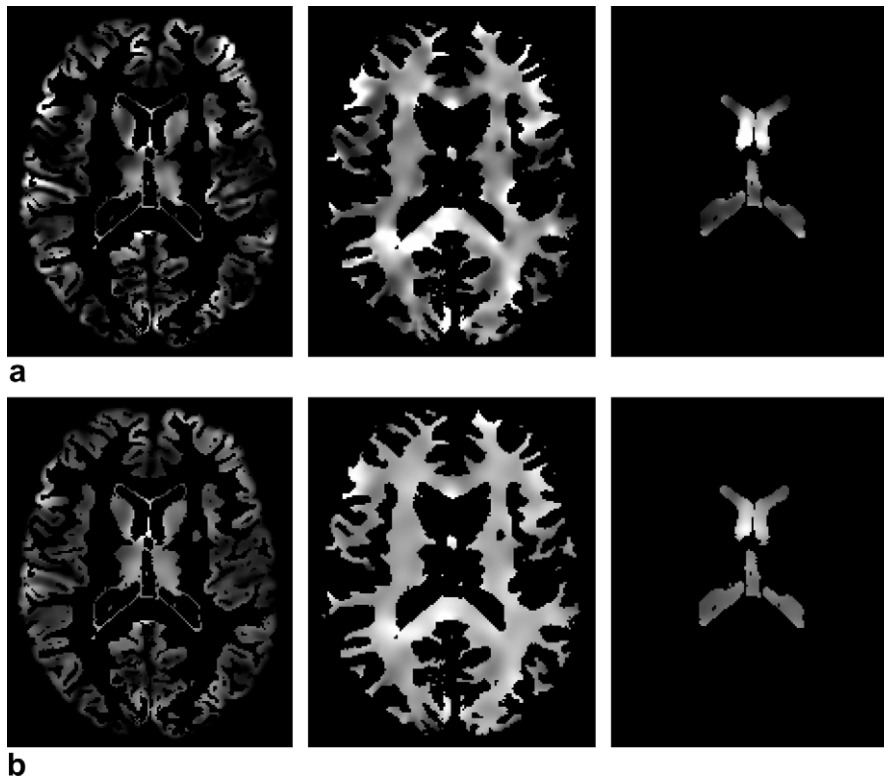


Fig. 10. Examples of the RAVENS maps for GM, WM and VN, calculated from the deformation fields generated by HAMMER and SMD+HAMMER, respectively. (a) HAMMER; (b) SMD+HAMMER.

Table 1

Paired *t*-test results: *p*-values and *t*-values at the peaks of clusters corresponding to the superior temporal gyrus and the precentral gyrus

	HAMMER	SMD+HAMMER
Cluster 1 (in the superior temporal gyrus)	$p_{\text{FWE-corr}} = 0.342$	$p_{\text{FWE-corr}} = 0.026$
	$p_{\text{FDR-corr}} = 0.057$	$p_{\text{FDR-corr}} = 0.003$
	$T = 12.91$	$T = 17.50$
Cluster 2 (in the precentral gyrus)	$p_{\text{FWE-corr}} = 0.272$	$p_{\text{FWE-corr}} = 0.003$
	$p_{\text{FDR-corr}} = 0.057$	$p_{\text{FDR-corr}} = 0.003$
	$T = 13.26$	$T = 22.29$

images have to be subjected to SMD regularization. Finally, we notice that these results are comparable to the inter-rater errors in placing landmarks, *i.e.* the mean and std are 5.6 and 3.6 mm, respectively, for the same testing data (with voxel size of $1 \text{ mm} \times 1 \text{ mm} \times 2.2 \text{ mm}$) (Xue et al., 2004).

3.2.2.2. Registering serial MR brain images. In this experiment, serial images of six different subjects from the BLSA project (Resnick et al., 2000) are registered onto the template image by HAMMER and SMD+HAMMER, respectively, to compare the goodness of registration. In the experiment, each subject has eight serial images captured from eight consecutive years. For accurately measuring the subtle longitudinal changes, it is important to evaluate the temporal consistency of the registration results on the

serial images of each subject. Therefore, the temporal smoothness (TS) of the T serial deformation fields, used to register the serial images of the same subject to the template, is measured,

$$\text{TS}(\mathbf{x}) = \frac{1}{T-2} \sum_{t=2}^{T-1} \left| \mathbf{f}_t(\mathbf{x}) - \frac{\mathbf{f}_{t+1}(\mathbf{x}) + \mathbf{f}_{t-1}(\mathbf{x})}{2} \right|. \quad (8)$$

A smaller TS value at \mathbf{x} means the deformation fields along the corresponding voxels of \mathbf{x} in the serial images are temporally smooth, while a large TS value means that deformation fields are not temporally smooth. Notice that temporal consistency or temporal smoothness is an important indicator of method robustness in many studies, in which relatively small brain changes are known to have occurred between consecutive scans. Here, we exploit this fact to test the stability and robustness of our registration method. Fig. 12 gives an example of the TS map. Fig. 12(a) shows the TS map calculated from the serial deformation fields generated by using HAMMER, and Fig. 12(b) gives the TS map by using SMD+HAMMER. It can be seen that the TS map in Fig. 12(b) has smaller values than that in Fig. 12(a), *e.g.* smaller peaks and lower peak values are observed. We can also calculate the difference between the TS map of SMD+HAMMER and that of HAMMER, and overlay this difference of TS maps upon the template image, as shown in Fig. 12(c). According to the color bar, we can observe that SMD+HAMMER can achieve better results within the red regions and similar results within the yellow regions.

In fact, most values in the difference of TS maps are negative, indicating that SMD+HAMMER generates temporally smoother serial deformation fields for the serial images than HAMMER. Alternatively, we can calculate the histogram of the difference of TS maps, to see whether SMD+HAMMER improves the temporal smoothness. Fig. 13 shows six such histograms for six different subjects. It can be seen that for each subject, most values of the difference of the TS maps are below zero, thus most TS values of SMD+HAMMER are smaller than those of

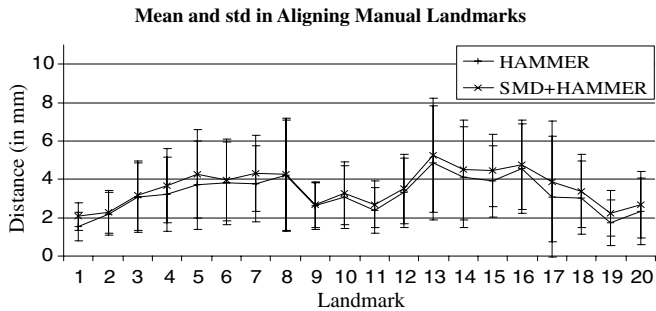


Fig. 11. Comparison of the registration accuracy on manual landmarks.

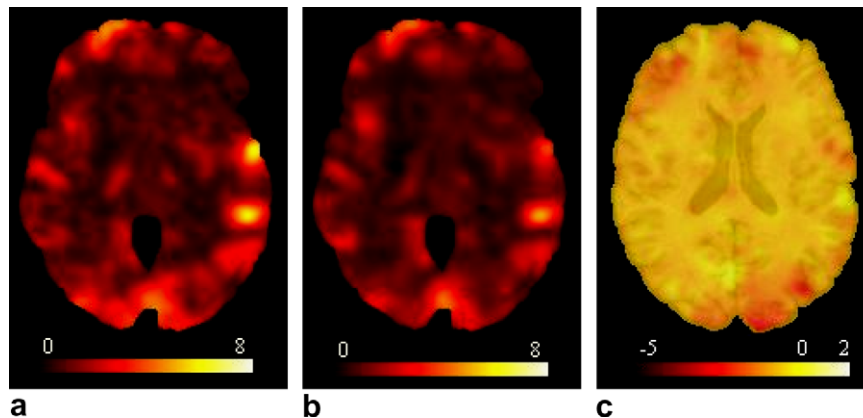


Fig. 12. Comparison of temporal smoothness of serial deformation fields. The difference of TS maps is defined as the subtraction of the TS map of SMD+HAMMER by the TS map of HAMMER. (a) HAMMER; (b) SMD+HAMMER; (c) overlaying the difference of TS maps upon the template image.

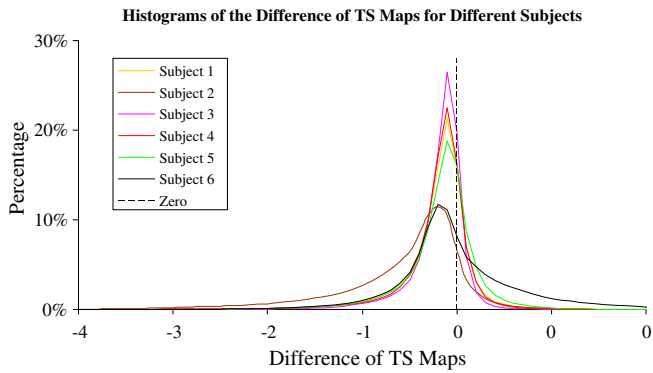


Fig. 13. Histograms of the difference of TS maps for six different subjects.

HAMMER. Thus, compared to HAMMER, SMD+HAMMER produces temporally smoother registration results for serial images.

The temporally consistent registration results by SMD+HAMMER can be also visually observed via 3D rendering. Fig. 14 shows the template image and the registered serial images of the same subject in the template space, using a 3D rendering, for HAMMER and SMD+HAMMER, respectively. White contours are identically placed in each image, for facilitating the visual inspection. It can be seen that the shapes of the deformed gyri for the year 1, year 3 and year 5 of the HAMMER registration results (indicated by black arrows in Fig. 14(b))

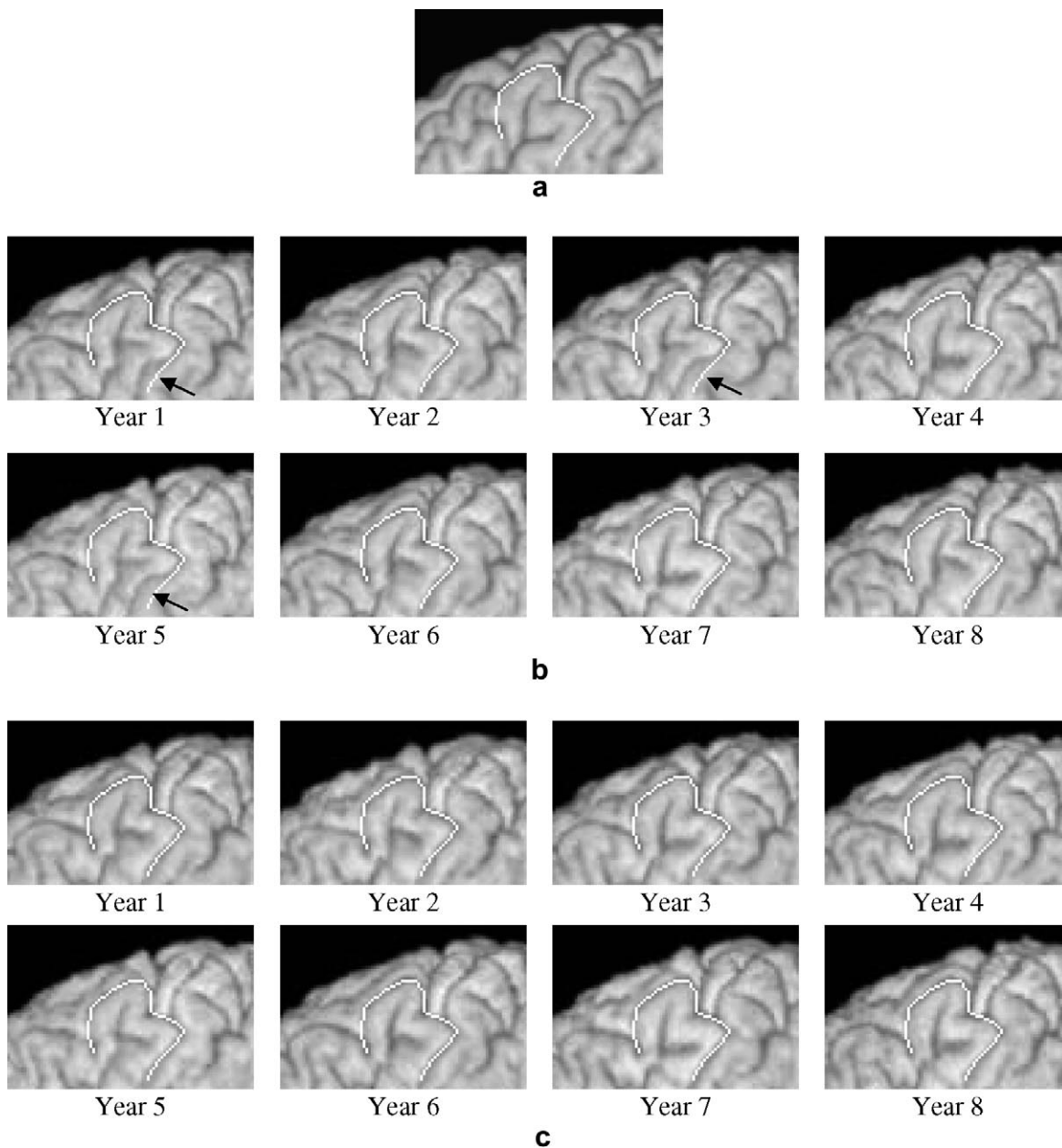


Fig. 14. Warping consistency on eight-year serial images of the same subject. (a) Template image; (b) registered serial images by HAMMER; (c) registered serial images by SMD+HAMMER.

are quite different from those in the other years. In contrast, the shapes of the registered gyri by SMD+HAMMER are not only more temporally consistent, but also more similar with the template as shown in Fig. 14(c).

4. Conclusion

A statistical model of deformation (SMD) is proposed in this paper to capture the statistics of high-dimensional deformation fields effectively. SMD uses the W-PCA model to estimate the pdf of high-dimensional deformation fields and represents the space of valid deformation fields as an intersection of three subspaces that reflect different aspects of deformation fields, *i.e.* W-PCA model of deformation fields, W-PCA model of Jacobian determinants of deformation fields, and a nested MRF smoothness regularization. Compared to the conventional statistical shape models, such as the active shape model (ASM), SMD can capture the statistics more accurately and effectively, especially for high-dimensional data and small sample sets. SMD is further used as the prior knowledge to regularize the deformation fields in an SMD-constrained registration framework. Experiments demonstrate that more robust registration results are obtained by the SMD-constrained registration, without decreasing the registration accuracy. Therefore, SMD can potentially be incorporated into various registration algorithms to improve their robustness and stabilities via statistically based regularization.

References

- Ashburner, J., Friston, K.J., 2000. Voxel-based morphometry: the methods. *Neuroimage* 11, 805–821.
- Belge, M., Kilmer, M., Miller, E., 2000. Wavelet domain image restoration with adaptive edge-preserving regularization. *IEEE Trans. Image Process.* 9, 597–608.
- Boesen, K., Frey, S., Huang, J., Germann, J., Stern, J., Collins, D.L., Evans, A.C., Rottenberg, D., 2005. Inter-rater Reproducibility of 3D Cortical and Subcortical Landmark Points. In: 11th Annual Meeting of the Organization for Human Brain Mapping, Toronto, Canada, 2005.
- Coifman, R.R., Wickerhauser, M.V., 1992. Entropy-based algorithms for best basis selection. *IEEE Trans. Inf. Theory* 38, 713–718.
- Cootes, T.F., Hill, A., Taylor, C.J., Haslam, J., 1994. Use of active shape models for locating structures in medical images. *Image Vision Comput.* 12, 355–365.
- Cootes, T.F., Taylor, C., Cooper, D., Graham, J., 1995. Active shape models – their training and application. *Comput. Vis. Image Und.* 61, 38–59.
- Cootes, T., Edwards, G., Taylor, C., 1998. Active appearance models. In: Fifth European Conference on Computer Vision, Freiburg, Germany, 1998.
- Davatzikos, C., 1998. Mapping of image data to stereotaxic spaces. *Human Brain Mapp.* 6, 334–338.
- Davatzikos, C., Genc, A., Xu, D., Resnick, S.M., 2001. Voxel-based morphometry using the RAVENS maps: methods and validation using simulated longitudinal atrophy. *NeuroImage* 14, 1361–1369.
- Davatzikos, C., Tao, X., Shen, D.G., 2003a. Hierarchical active shape models using the wavelet transform. *IEEE Trans. Med. Imaging* 22, 414–423.
- Davatzikos, C., Tao, X., Shen, D., 2003. Applications of wavelets in morphometric analysis of medical images. In: *SPIE Wavelets X*, San Diego, CA, 2003.
- Geman, S., Geman, D., 1984. Stochastic relaxation Gibbs distributions and Bayesian restoration of images. *IEEE Trans. Patt. Anal. Mach. Intell.* PAMI-6, 721–741.
- Goldszal, A.F., Davatzikos, C., Pham, D., Yan, M., Bryan, R.N., Resnick, S.M., 1998. An image processing protocol for the analysis of MR images from an elderly population. *J. Comput. Assist. Tomo.* 22, 827–837.
- Karacali, B., Davatzikos, C., 2004. Estimating topology preserving and smooth displacement fields. *IEEE Trans. Med. Imaging* 23, 868–880.
- Mallat, S., 1998. *A Wavelet Tour of Signal Processing*. Academic Press.
- Miller, M., Banerjee, A., Christensen, G., Joshi, S., Khaneja, N., Grenander, U., Matejic, L., 1997. Statistical methods in computational anatomy. *Stat. Method Med. Res.* 6, 267–299.
- Moghaddam, B., Pentland, A., 1997. Probabilistic visual learning for object representation. *IEEE Trans. Patt. Anal. Mach. Intell.* 19, 696–710.
- Mohamed, A., Davatzikos, C., 2004. Shape representation via best orthogonal basis selection. In: *Medical Image Computing and Computer Assisted Intervention (MICCAI)*, St. Malo, France, 2004.
- Resnick, S.M., Goldszal, A., Davatzikos, C., Golski, S., Kraut, M.A., Metter, E.J., Bryan, R.N., Zonderman, A.B., 2000. One-year age changes in MRI brain volumes in older adults. *Cereb. Cortex* 10, 464–472.
- Shen, D., Davatzikos, C., 2002. HAMMER: hierarchical attribute matching mechanism for elastic registration. *IEEE Trans. Med. Imaging* 21, 1421–1439.
- Shen, D., Ip, H., 1998. Markov random field regularization models for adaptive binarization of nonuniform images. *IEE Proc. Vis. Image Signal Process.* 145, 322–332.
- Staib, L.H., Duncan, J.S., 1992. Boundary finding with parametrically deformable models. *IEEE Trans. Patt. Anal. Mach. Intell.* 14, 1061–1075.
- Styner, M.A., Rajamani, K.T., Nolte, L.P., Zsemlye, G., Szekely, G., Taylor, C.J., Davies, R.H., 2003. Evaluation of 3D correspondence methods for model building. In: *Information Processing in Medical Imaging*, Ambleside, UK, 2003.
- Twining, C.J., Cootes, T., Marsland, S., Petrovic, V., Schestowitz, R., Taylor, C.J., 2005. A unified information-theoretic approach to groupwise non-rigid registration and model building. In: *Information Processing in Medical Imaging*, Glenwood Springs, CO, 2005.
- Xue, Z., Shen, D., Davatzikos, C., 2004. Determining correspondence in 3D MR brain images using attribute vectors as morphological signatures of voxels. *IEEE Trans. Med. Imaging* 23, 1276–1291.
- Xue, Z., Shen, D., Karacali, B., Davatzikos, C., 2005. Statistical representation and simulation of high-dimensional deformations: application to synthesizing brain deformations. In: *Medical Image Computing and Computer Assisted Intervention (MICCAI 2005)*, Palm Springs, CA, USA, 2005.